Geomechanics and Engineering, *Vol. 35, No. 1 (2023) 1-11*
https://doi.org/10.12989/gae.2023.35.1.001

Estimating the lateral profile of helical piles using modified *p-y* springs

Hyeong-Joo Kim[1a], Hyeong-Soo Kim*[2], Peter Rey Dinoy[3b], James Vincent Reyes[2c], Yeong-Seong Jeong[2d], Jun-Yong Park[2e] and Kevin Bagas Arifki Mawuntu[2f]

[1]*Department of Civil Engineering, Kunsan National University, 558 Daehak-ro, Miryong-dong, Gunsan 54150, Republic of Korea*
[2]*Department of Civil and Environmental Engineering, Kunsan National University, 558 Daehak-ro, Miryong-dong, Gunsan 54150, Republic of Korea*
[3]*Renewable Energy Research Institute, Kunsan National University, 558 Daehak-ro, Miryong-dong, Gunsan 54150, Republic of Korea*

(*Received November 25, 2022, Revised August 3, 2023, Accepted August 12, 2023*)

Abstract. A growing trend of utilizing helical piles for soft soil strata to support infrastructure projects is currently observed in Saemangeum, South Korea. Recognized mainly due to its ease of installation and reusability proves to be far more superior compared to other foundation types in terms of sustainability. This study applies modified p-y springs to characterize the behavior of a laterally loaded helical pile with a shaft diameter of 89.1 mm affixed with 3 helices evenly spaced along its embedded length of 2.5 m. Geotechnical soil properties are correlated from CPT data near the test bed vicinity and strain gauges mounted on the shaft surface. A modification factor is applied on the p-y springs to adjust the simulated data and match it to the bending moment, soil resistance and deflection values from the strain gauge measurements. The predicted lateral behavior of the helical pile through the numerical analysis method shows fairly good agreement to the recorded field test results.

Keywords: CPT; helical piles; instrumented piles; p-y springs; static lateral load test

1. Introduction

Oil and coal have generally been used to generate power since the early years of the industrial revolution. Soon, these natural resources will eventually deplete, and environmentally friendly alternatives such as wind and sunlight will be sourced due to their eternal nature. Currently, the government is investing in various onshore photovoltaic projects (also known as solar farms) to utilize the reclaimed areas in Saemangeum, South Korea. Since the project is to be built on soft reclaimed soil, helical piles were chosen as foundation alternatives to traditional concrete pads and piles for the following reasons: the unique feature of having helices along its shaft facilitates ease of installation and removal, as mentioned by Brown *et al.* (2019); they provide more considerable uplift and compressive capacity due to the helix bearing area, as mentioned by Spagnoli (2020); economic usage for soil conditions with high groundwater table, as mentioned by Vignesh and Mayakrishnan (2020); and concrete pads are prone to differential settlement that leads to a tilting effect, as mentioned by Kim *et al.* (2021) and Seo *et al*. (2022).

Concrete disposal also presents an environmental issue after the decommissioning or relocation of the structure. In contrast, the helical piles can still be reused, justifying their usage as an alternative foundation for sustainable development venture projects.

Authors such as Puri *et al*. (1984), Prasad and Narasimha Rao (1996), Sakr (2009, 2018), Mittal *et al.* (2010), Abdrabbo and Wakil (2016), Dave and Soni (2019) and Sinha *et al.* (2021) conducted extensive research on the lateral behavior of helical piles through full-scale field tests and developed mathematical models to estimate the lateral capacity of a specific helical pile configuration. Their research findings suggest that helical piles mobilize more excellent lateral resistance than regular shaft piles. Their mathematical models predicted results in good agreement compared to the field test results. A Ph.D. dissertation done by Elkasabgy (2011) first proposed the p-y approach by numerical analysis of the lateral capacity of helical piles using the LPILE program followed by Li and Yang (2017) and by Elkasabgy and El Naggar (2019). The p-y approach is much more preferred than the conventional field test as it describes the lateral profile per depth (bending moment, soil resistance, slope curvature, and pile deflection) rather than just the measured pile head deflection of the latter.

Aside from quantifying the lateral behavior of helical piles, examining the internal forces along the pile is essential to determine whether the material's mechanical properties and cross-section are enough to carry the design loads. Usually, piles are designed to carry a combination of axial and lateral loads (Khari *et al.* 2021) but focus on the lateral aspect of the helical piles is explored in this paper. Lateral forces are mainly generated by exposure to environmental loads such as wind gusts, which result in extreme overturning moments the pile must withstand.

*Corresponding author, Post Doc Researcher
E-mail: gudtn3004@kunsan.ac.kr
[a]Professor
[b]Ph.D.
[c]Graduate Student
[d]Graduate Student
[e]Graduate Student
[f]Graduate Student

ISSN: 2005-307X (Print), 2092-6219 (Online)

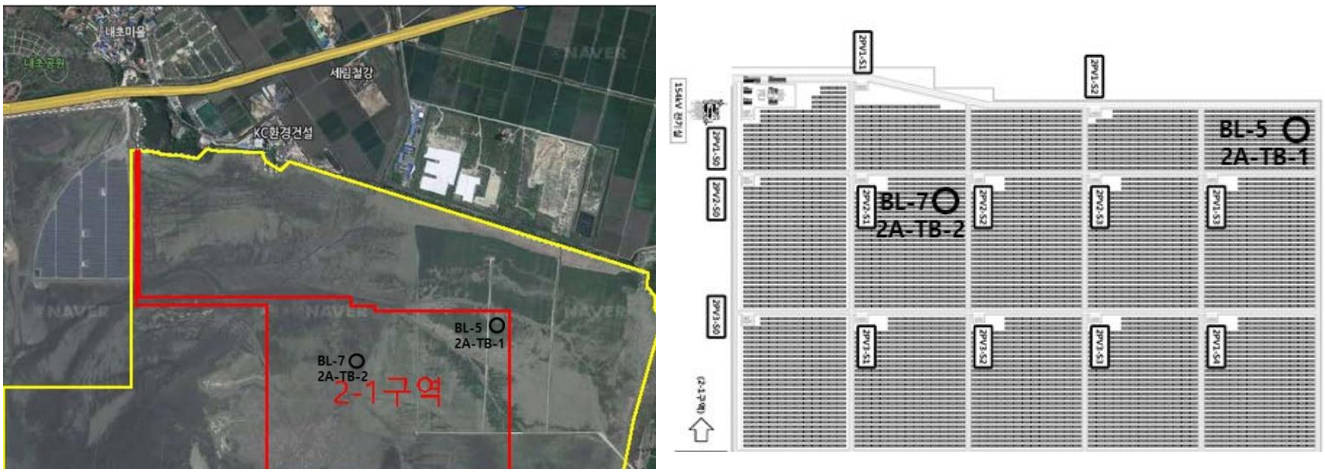

(a) Satellite view (b) CAD view of research site

Fig. 1. Test bed area

Accurately evaluating the developed internal forces will result in an efficient and cost-friendly design (Kim *et al.* 2022) that will generally contribute to the project's sustainability goal.

This paper examines the developed internal forces generated along the embedded pile length when the pile head is subjected to static lateral loads. Regular helical piles widely applied in the industry have a helix-to-pile shaft diameter ratio (D_h/D_p) of less than three and a total embedment depth to first helix embedment depth ratio (L/z_h) of less than two are commonly presented in various research studies. This study investigates the behavior of a laterally loaded helical pile with a D_h/D_p ratio of 4.5 (greater than three) and an L/z_h ratio of 5 (greater than two).

The measured strains from a full-scale instrumented helical pile is converted to bending moment and soil resistance values and compared to the numerically simulated results using the modified p-y springs method.

The theoretical p-y springs method from an earlier study by Kim *et al.* (2022) incorporates the added lateral resistance from the helix plates to the pile's overall lateral capacity. The soil geotechnical properties are correlated from gathered CPT data in the test field.

2. Subsurface Investigation

The area shown in Fig. 1 is part of the South Korean government's proposed 300 MW Onshore Solar Power Generation Project in the Saemangeum area of Jeollabuk-do province. Two sets of Cone Penetration Tests (CPT) for a depth up to 10.30 m below the ground surface were conducted at the test bed area labeled BL-5 and BL-7. Aside from the two CPT soundings, six boreholes were also commissioned to collect SPT data at the research area with penetration depths varying from 25.50 m to 32.50 m. Also, disturbed and partially disturbed soil samples were collected for routine laboratory tests such as water content determination and sieve analysis. Shown in Figs. 2 and 3 are the CPT data of BL-5 and BL-7, respectively. According to the Guide of Cone Penetration Testing, CPT cannot provide accurate predictions of the physical characteristics of soils but rather offer a reliable guide to its mechanical properties and soil behavior type (SBT). Shown in Figs. 2(h) and 3(h) are the corresponding soil behavior type of BL-5 and BL-7, estimated from the CPT data and processed in a commercial geotechnical correlation software, NovoCPT. The soil behavior type shows that the first 1.50m profile of BL-5 mostly behaves as a combination of silty clay to clay and sandy silt to clayey silt followed by a layer of silty clay to clay until a depth of 2.1m. In contrast, the first 1.50 m profile of BL-7 is sandy silt to silty sand, which can be approximated as a sandy layer followed by a clay layer until a depth of 2.5 m. Both, however, share the same ground water table level observed at a depth of 0.7m below the ground surface.

For the numerical simulation, only the soil properties of BL-7 area is considered since the strain gauges of area BL-5 are not usable and the measured helical pile profile cannot be compared. In BL-7, the embedment depth of 2.5 m was determined to be two layers of different soils; the first 1.5 m was a sandy layer, while the remaining depth was approximated to be a soft clay layer. The first layer had an equivalent SPT $(N_1)_{60}$ value of 8, which was classified as an equivalent silty sand layer by the SBT chart. In contrast, the second layer had an equivalent SPT $(N_1)_{60}$ value of 2, which was classified as an equivalent clay layer. For the first layer, the p-y curve from Reese *et al.* (1974) determined the soil layer type being sandy soil, while for layer two, the p-y curve of Matlock (1960) was chosen to represent the clay layer. The unit weight for both soil layers was determined by using Eq. (1) (Robertson 2010), since the soil layer in the test bed had a 0.7 m groundwater table, the effective unit weight was taken for analysis

$$\frac{\gamma}{\gamma_w} = 0.27[\log R_f] + 0.36\left[\log\left(\frac{q_t}{p_a}\right)\right] + 1.236 \quad (1)$$

where R_f is the friction ratio $[(f_s/q_t)x100]$, γ_w is the unit weight of water, and p_a is the atmospheric pressure

$$S_u = \frac{q_t - \sigma_v}{N_{kt}} \quad (2)$$

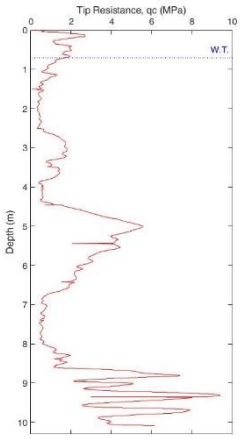

(a) Tip Resistance, qc

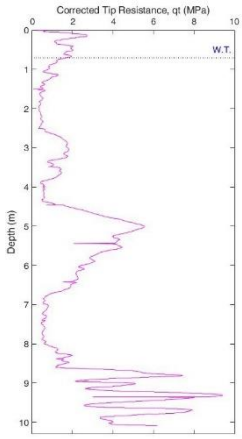

(b) Corrected Tip Resistance, qt

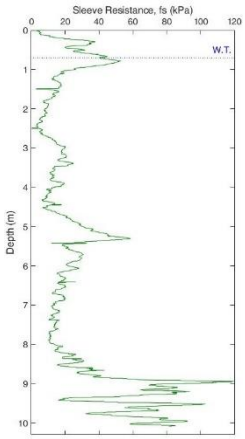

(c) Sleeve Resistance, fs

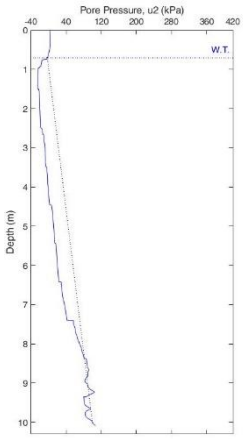

(d) Pore Pressure, u_2

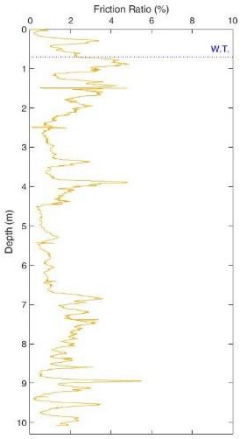

(e) Friction Ratio

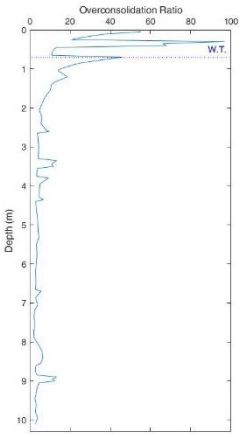

(f) Overconsolidation Ratio

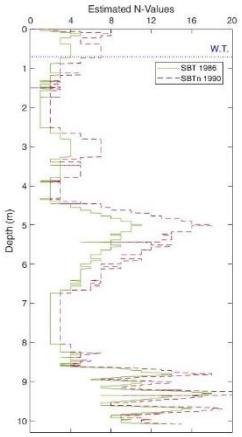

(g) Estimated N-Values

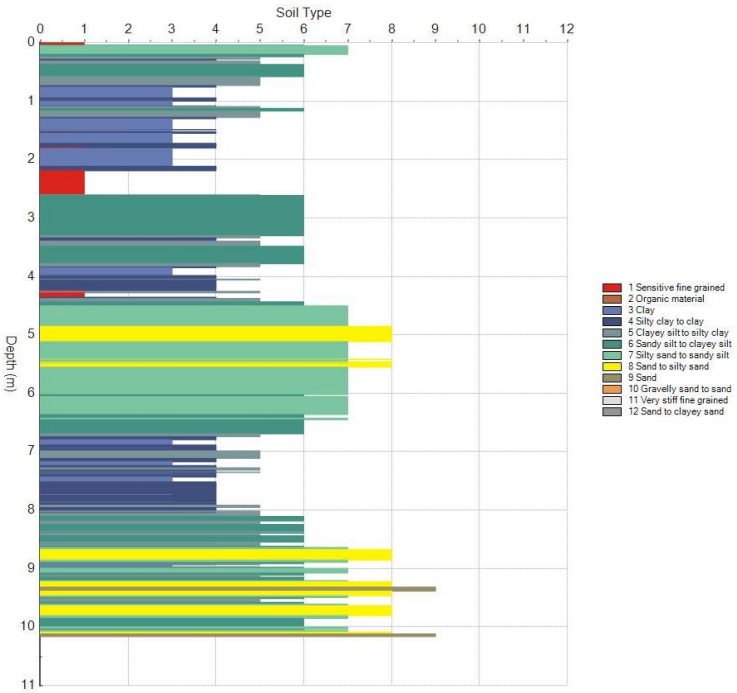

(h) Soil Behavior Type (SBT)

Fig. 2 Geotechnical parameters for site BL-5

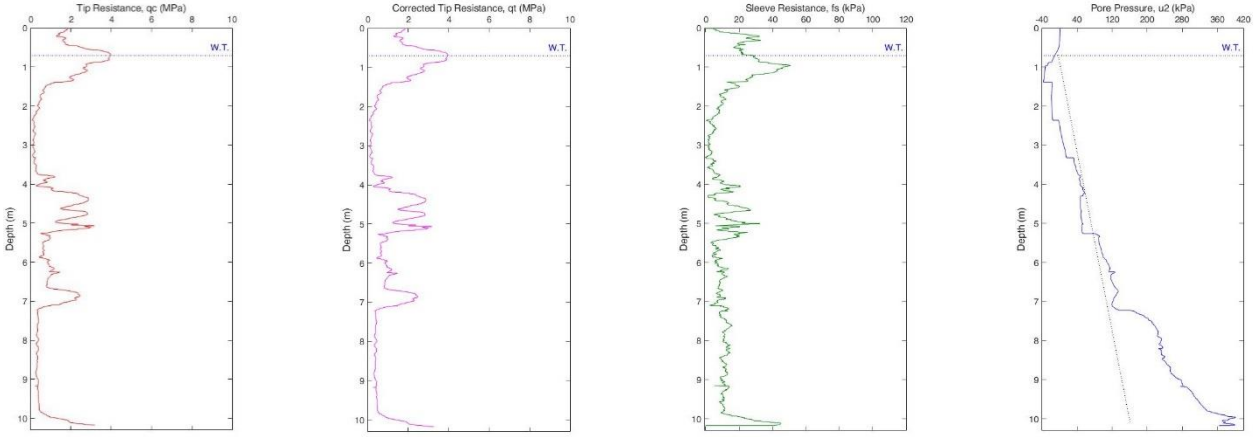

(a) Tip Resistance, qc (b) Corrected Tip Resistance, qt (c) Sleeve Resistance, fs (d) Pore Pressure, u_2

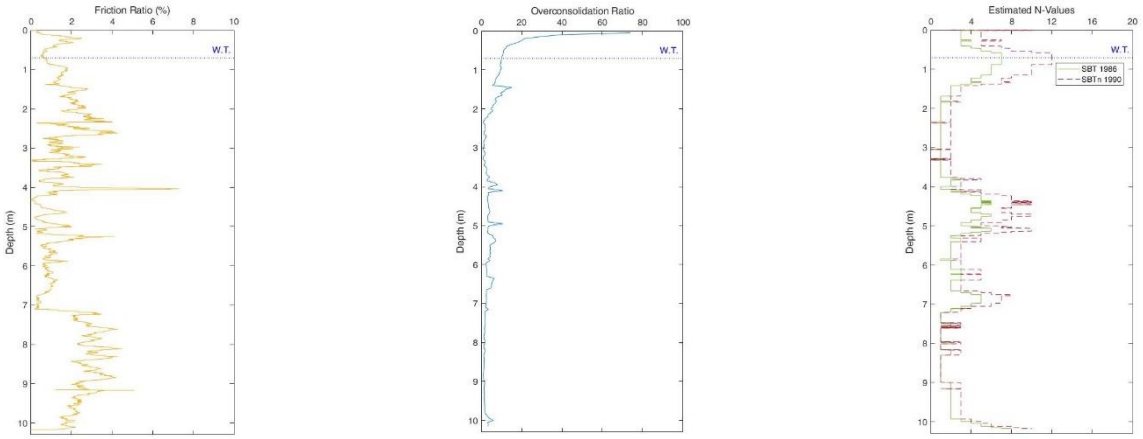

(e) Friction Ratio (f) Overconsolidation Ratio (g) Estimated N-Values

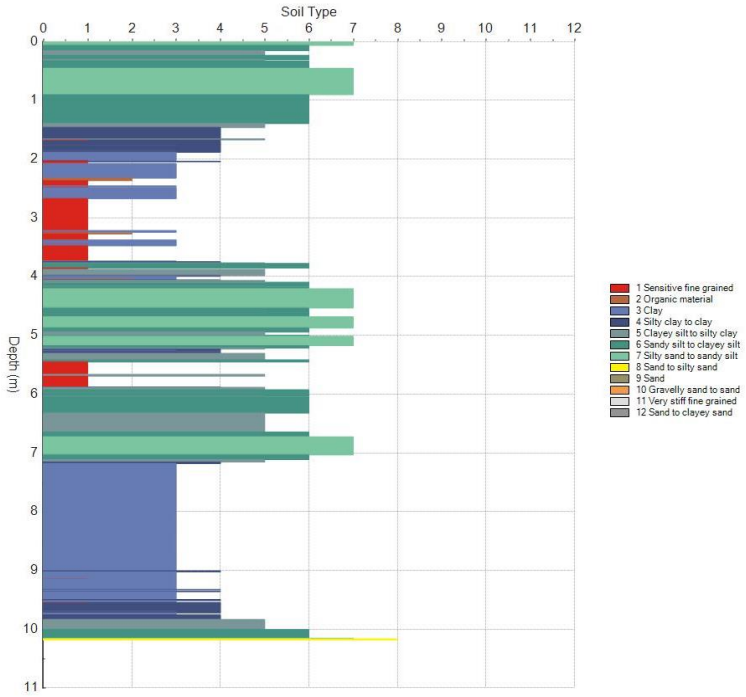

(h) Soil Behavior Type (SBT)

Fig. 3 Geotechnical parameters for site BL-7

where q_t is the corrected tip resistance, σ_v is the overburden pressure, and N_{kt} is the preliminary cone factor (adopted the average coefficient value of 14 for the correlations)

$$\phi = \sqrt{20(N_1)_{60}} + 20 \quad (3)$$

The undrained shear strength of clay was determined using Eq. (2) (Robertson 2010). The soil friction angle for sandy soils was taken from Eq. (3) (Hatanaka and Uchida 1996) using the equivalent SPT $(N_1)_{60}$ value estimated from CPT. The selection soil friction angle is based on the designer's preference and discretion as mentioned by Sancak and Cinicioglu (2020), in this analysis, the peak soil friction angle is used. The ε_{50} values were taken from the LPile Technical Manual, which has representative values for each clay consistency. The empirical constant (J) was provided by Matlock (1970) to have a value equal to 0.5 for soft clays and 0.25 for medium clay. The empirical constant used in this study is 0.5 since the clay soil in the test field was observed to be soft clay and proven by the conducted routine soil experiments in the laboratory.

3. Lateral load test and pile instrumentation

The acceptance criteria for helical pile foundations follow the established general requirements for deep foundations as stated by the Acceptance Criteria for Helical Pile Foundations, Systems and Devices (AC358). The lateral load tests were conducted in compliance with Procedure A (Standard Loading) and following the technical specifications stated in ASTM D3966-07 (ASTM, 2007), Standard Test Methods for Deep Foundations Under Lateral Loading.

The laterally loaded helical piles have a shaft diameter of 89.1 mm and 3.2 mm thickness, with three helices welded onto the central shaft having 400 mm, 200 mm, and 200 mm diameters, respectively as shown in Fig. 4. The first helix is located 0.7 m below the pile head, and the succeeding helices are spaced 0.9m apart. The helical test piles have a total length of 2.7 m, an embedment depth of 2.5 m, and the pile head is 0.2 m above ground. The helical piles were spaced 2.5 m apart center to center longitudinally from each other and 2.5 m laterally from the reaction piles. The same test set-up was conducted for both BL-5 and BL-7 test sites. Reaction piles have an embedment length of 3.0 m with a 0.5 m protruding portion for a total of 3.5 m, have a central shaft diameter of 139.8 mm and a thickness of 4.5 mm, fitted with 3-400 mm diameter helices with 4.0 mm thickness spaced at 1.0 m intervals along its length. The steel material used in manufacturing the helical pile shaft and reaction piles has a yield strength of 355 MPa and modulus of elasticity of 210 GPa. The load applied on the pile head was monitored by an electronic load cell with 300 kN capacity and delivered by a hydraulic jack at approximately 0.1 m above the ground surface. To measure the displacement of the pile head, one LVDT (linear variable differential transformer) with 0.01 mm accuracy and 150 mm travel distance was attached to the opposite side of the pile head parallel to the load direction. All field data were collected using an electronic data logger and monitored by personnel on site. The static pile head loads were applied in increments where each increment was maintained

Table 1 Geometrical properties of test and reaction piles

	Test Pile	Reaction Pile
Embedment ratio, L/L_e	1.08	1.17
Inter-helix spacing ratio, S/D_h	3.0 (1-2) 4.5 (2-3)	2.5 (1-2) 2.5 (2-3)
Helix to shaft ratio, D_h/D_p	4.5 (1-2) 2.2 (2-3)	2.9 (1-2) 2.9 (2-3)

Note L = total pile length; L_e = embedment length; S = inter-helix spacing; D_h = helix diameter; D_p = pile shaft diameter (1-2) represents the first helix and the second helix (2-3) represents the second helix and the third helix

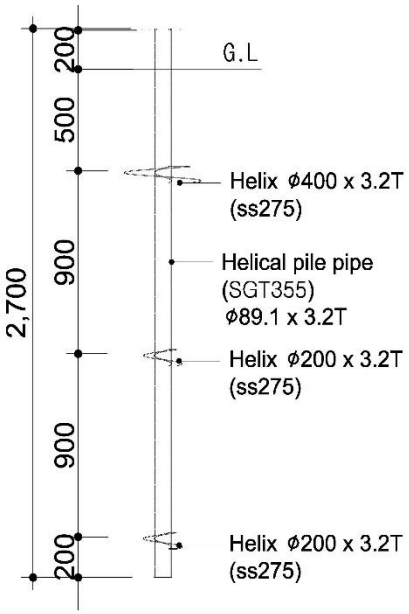

Fig. 4 Helical pile CAD

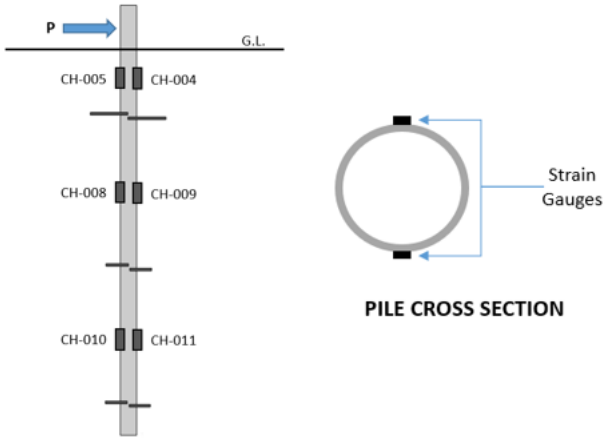

Fig. 5 Strain gauge instrumentation set-up

for a period of five minutes. A total of 9 and 4 load steps (increments) were applied during the loading and unloading phase, respectively and the whole test duration was 65 minutes.

The helical test piles were instrumented with three pairs of electrical resistance-type strain gauges on diametrical opposites along the embedded shaft length. The 60 mm longitudinal gauge length is parallel to the shaft length and is aligned perpendicular to the application of loads to measure the bending strains developed during loading. Shown in Fig. 5, the point of application of lateral loads is at the left side of the pile

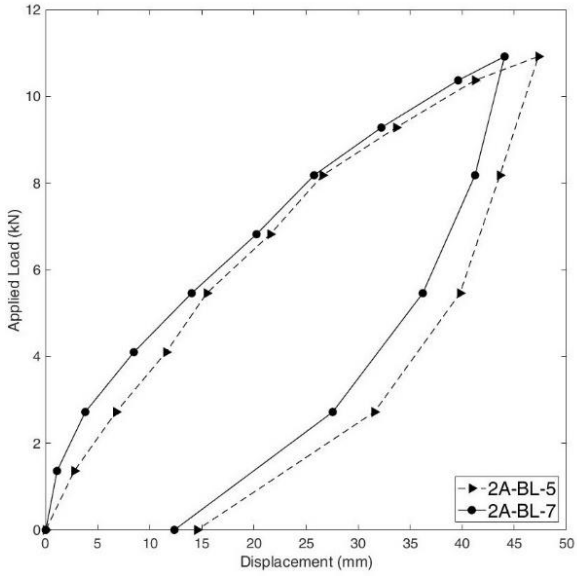

Fig. 6 Field test load-displacement graph

where strain gauges CH-005, CH-008, and CH-010 are situated, while at the right side are strain gauges CH-004, CH-009, and CH-011. The strain gauges were installed on the outer surface diameter using a special-purpose adhesive. To ensure the survival of the strain gauges during pile installation, SB tape (butyl rubber) was placed above the strain gauges as the first coating, followed by another coating of VM (butyl rubber) tape. Protective tape was applied throughout its embedded length to ensure that the strain gauge wires would survive the installation phase. The raw strains generated during the load test were recorded using an electronic data logger and monitored on-site.

Raw strain readings show the positive and negative strains developed at the points where the gauges were located. Unfortunately, none of the strain gauges in the BL-5 test bed were working, hence strain data was unavailable. Only the strain gauges of the BL-7 test bed were usable. CH-005, CH-008, and CH-010 display positive strains due to the tensile behavior of the pile shaft, while CH-004, CH-009, and CH-011 display negative strains due to the compressive behavior exhibited by the pile shaft during flexure. The assumption of the pile bending profile proves to be correct, as verified by the strain readings recorded.

Shown in Fig. 6 is the lateral load-displacement graph for test areas BL-5 and BL-7. The graph displays the measured lateral displacements of the pile head corresponding to the applied static loads. As observed, the test result of area BL-5 is weaker than area BL-7, which backs up the soil type profile interpreted from the CPT tests and the tip resistance values between the two. The first few meters of BL-5 contain mostly soft clay soil type; the small values of corrected tip and sleeve resistance indicate a weak layer of cohesive soil properties that the pile depends on mobilizing strength. On the other hand, the soil type composition of BL-7 has a sand layer and relatively larger corrected tip and sleeve resistance values. It may not be much, but this influences the difference between the overall mobilized lateral capacity of the pile of the two test bed locations.

4. Numerical modeling and analysis

4.1. Modified p-y springs method

To numerically model the lateral behavior of the helical piles, this study employs the use of modified p-y springs established from an earlier study conducted by Kim *et al.* (2022). A laterally loaded helical pile is treated as a beam-column inserted in an elastic foundation. The soil is discretized as a series of independent non-linear springs that store the soil resistance and pile deflection values (p-y curve) as a function for each depth. The soil resistance values depend on the soil type and geotechnical properties. The soil resistance (p_s) value is computed using Eq. (4), where the minimum value between Eqs. 5(a) and 5(b) for sand and Eqs. 7(a) and 7(b) for soft clay is considered. For an in-depth understanding, the authors highly suggest referring to the work done by Reese *et al.* (1974) for sand and Matlock (1960) for soft clay which the p-y curve procedure is used to model the soil in this study. Once the soil resistance value is established, the springs within the zone of influence are applied with a soil resistance factor (P_{mult}) shown in Eq. (8) and the reinforced soil resistance value (p_{rs}) shown in Eq. (9), is used in the computation. Fig. 7 shows the concept of zone of influence of a helical plate and the p-multiplier distribution. The full value of the p-multiplier is applied at the center where the helix plate is located and gradually decreases in value to a minimum value of 1.0, which indicates that the boundary of the zone of influence of the helix plate is reached. The numerical solution is based on the fourth-order differential equation derived by Hetenyi (1946) and is solved using the finite difference method, coded using the commercial software MATLAB.

$$p_s = \min[p_a, p_b] \tag{4}$$

For sand,

$$P_a = \gamma z \left[\begin{array}{c} \dfrac{K_0 z \tan\phi \sin\beta}{\tan(\beta-\phi)\cos\alpha} \\ + \dfrac{\tan\beta}{\tan(\beta-\phi)}(b + z\tan\beta\tan\alpha) \\ + K_0 z \tan\beta(\tan\phi\sin\beta - \tan\alpha) - K_a b \end{array} \right] \tag{5a}$$

$$P_b = K_a b\gamma z(\tan^8\beta - 1) + K_0 b\gamma z \tan^4\beta \tag{5b}$$

$$\alpha = \frac{\phi}{2} \tag{6a}$$

$$\beta = 45 + \frac{\phi}{2} \tag{6b}$$

$$K_0 = 0.4 \tag{6c}$$

$$K_a = \tan^2\left(45 - \frac{\phi}{2}\right) \tag{6d}$$

where z represents the depth relative to the ground line and b is the pile shaft diameter. Best estimates of: friction angle, ϕ and soil unit weight, γ (for soils below water table, the

Table 2 Soil properties used to model the soil layer

						SAND			CLAY			
Depth (m)	Ave. N_{60}	Ave. $(N_1)_{60}$	SBT	SBT_n	p-y curve	ϕ	γ' (kN/m^3)	k_0	$S_u{}^a$ (kN/m^2)	γ' (kN/m^3)	$\varepsilon_{50}{}^b$	J^c
0.0 ~ 1.5	5	8	Silty Sand	6	Reese	33	8.4	0.4	-	-	-	-
1.5 ~ 2.5	1	2	Clay	3	Matlock	-	-	-	28.0	7.7	0.02	0.5

Note: [a] Undrained shear strength of clay, [b] Strain corresponding to one-half the maximum principal stress difference, [c] Matlock (1970) empirical constant; 0.5 for soft clays and 0.25 for medium clays

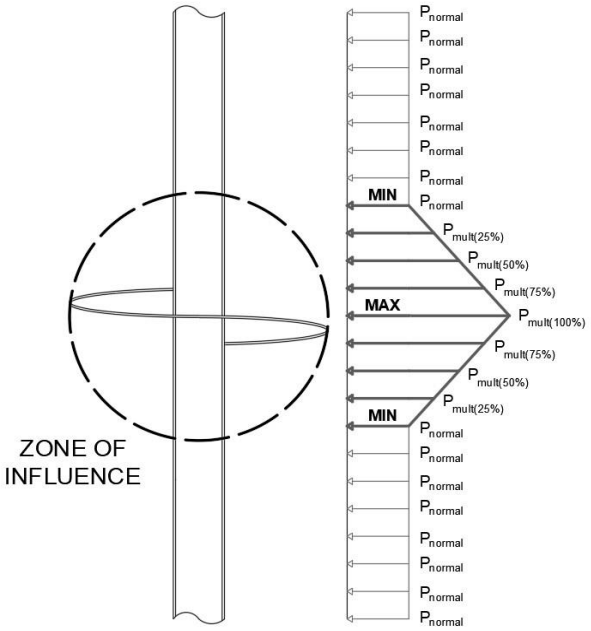

Fig. 7 Modified p-y springs concept by Kim *et al*. (2022)

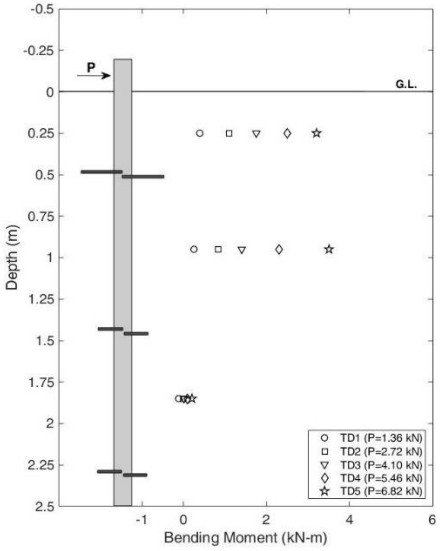

Fig. 8 Converted strains to bending moment

effective unit weight must be used; while for soil above water table, the total unit weight) are used in the analysis For soft clay,

$$P_a = cb\left[3 + \frac{\gamma z}{c} + \frac{Jz}{b}\right] \tag{7a}$$

$$P_b = 9cb \tag{7b}$$

where c is the shear strength, z represents the depth relative to the ground line and b is the pile shaft diameter and J is the empirical constant by Matlock (1970)

$$P_{mult} = \Omega\left(\frac{D_h - D_p}{D_p}\right) \tag{8}$$

where D_h is the helix plate diameter, D_p represents the pile shaft diameter, and Ω is the empirical pile coefficient

$$p_{rs} = P_{mult}(p_s) \tag{9}$$

4.3 Strain gauge interpretation

The bending moments developed along the pile shaft were determined by converting strain gauge readings using Eq. 10 to moment values that display the bending moment profile of a laterally loaded helical pile. Each moment value per depth corresponds to an applied load on the pile, as shown in Fig. 8.

$$M = (\varepsilon)\frac{EI}{y} \tag{10}$$

4.4 Polynomial approximation through curve-fitting

Based on the theory of a beam on an elastic foundation, the fundamental relationships between bending moment (M), soil resistance (p), and pile deflection (y) of a beam under constant flexural rigidity (EI) is given by Eqs. (11)-(13), respectively. The soil resistance is the double derivative of the bending moment, while the pile deflection is the double integral of the bending moment.

$$M = EI\frac{d^2M}{dx^2} \tag{11}$$

$$p = \frac{dV}{dx} = EI\frac{d^2M}{dx^2} = EI\frac{d^4y}{dx^4} \tag{12}$$

$$y = \frac{1}{EI}\iint M dx \tag{13}$$

A curve fitting procedure is used to approximate a laterally loaded pile's soil resistance distribution and deflection; a

fourth-order polynomial function curve is fitted to the bending moment profile. This curve-fitting procedure uses a similar approach to the experiments and studies conducted by authors Matlock and Ripperger (1956), Nip and Ng (2005) and Rathod *et al*. (2018). To obtain the soil resistance along the pile shaft, the bending moment function from curve fitting (Eq. (14)) is doubly differentiated, which yields the form in (Eq. (15)). And to obtain the deflection profile along the pile length, the bending moment function (Eq. (14)) is doubly integrated which yields the form displayed in (Eq. (16)). As a consequence of integration, two constants are produced during the process (C_1, and C_2). The value of these constants can be obtained from the pile boundary conditions. As each load produces its distinct moment curve profiles (i.e., the value and location of the maximum moment is a function dependent on the applied load), values for the integrating constants vary. Therefore, differentiations and integrations were done accordingly for all loading cases. The values from the field experiment will be cross-referenced with a simulated numerical model with the same parameters

$$M(x) = ax^4 + bx^3 + cx^2 + dx + e \tag{14}$$

where x is the depth below the pile head; a, b, c, d, e are the curve fitting constants

$$p = 12ax^2 + 6bx + 2c \tag{15}$$

$$y(x) = \frac{1}{EI}\left(\frac{a}{30}x^6 + \frac{b}{20}x^5 + \frac{c}{12}x^4 + \frac{d}{6}x^3 + \frac{e}{2}x^2 + C_1x + C_2\right) \tag{16}$$

4.5 Empirical pile coefficient used in simulation

The helix coefficient for this study was determined to be a value equal to 1.3 from visual examination of the comparison between the simulated data with no P_{mult}, simulated data with P_{mult}, and field test data. As displayed in Fig. 10, the difference can be seen in that a P_{mult} is needed to adjust the simulated data to match the field test displacement results. The helix coefficient value was adjusted from 1.0 until a match of 1.3 was reached. For each value adjustment, points were graphed and examined if they touched the field test results curve. The best fit value was determined to be 1.3, as values lower or higher would produce unsatisfactory load-displacement plots.

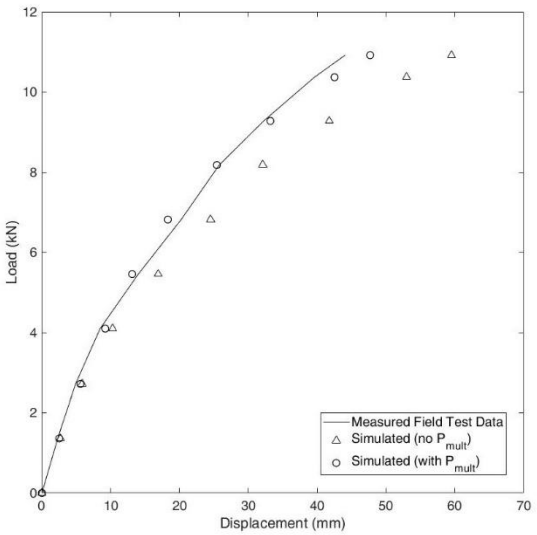

Fig. 9 Simulated vs. measured pile head displacements

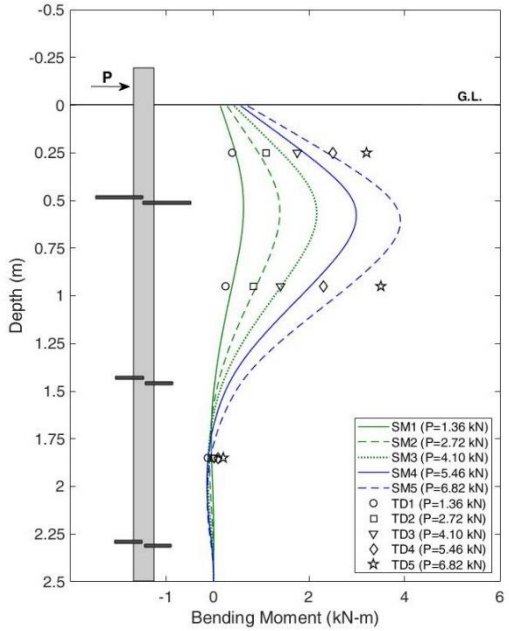

Fig. 10 Simulated vs. measured pile bending moment

5. Results and discussion

For a shaft diameter of 89.1 mm with a thickness of 3.2 mm and a yield strength of 355 MPa, the ultimate elastic moment capacity and the plastic moment capacity is 5.72 kN-m and 7.55 kN-m respectively (considering a reduction factor of 0.9). The elastic limit is reached when a lateral load of 7.66 kN is applied, loads beyond this is already on the plastic region. One of the assumptions in deriving the differential equation for the p-y analysis is that the pile material must remain in its elastic region and must not exceed its proportional limit. Hence, for this study, loads beyond 7.66 kN are discarded.

Figs. 10 and 11 shows the comparison between the simulated and measured values of the bending moment and soil resistance, respectively. As shown, the simulated data shows a fairly reliable predicted behavior compared to the measured test data which was converted from the strain gauge readings.

The maximum bending moment generated in the helical pile is observed to be around the range of 0.5 m ~ 0.6 m below the ground line (depending on the applied pile head loading).

This can be explained by the presence of the helix plate in the region. The helix plate acts as an intermediate lateral stiffener on the pile shaft as it resists pile movement by resisting in compression to the soil on its contact surfaces. Since the movement of the shaft is partially restricted, this allows the region to condense larger internal forces before translating and transferring the excess forces further along the shaft length. For a regular shaft pile, the shaft continuously

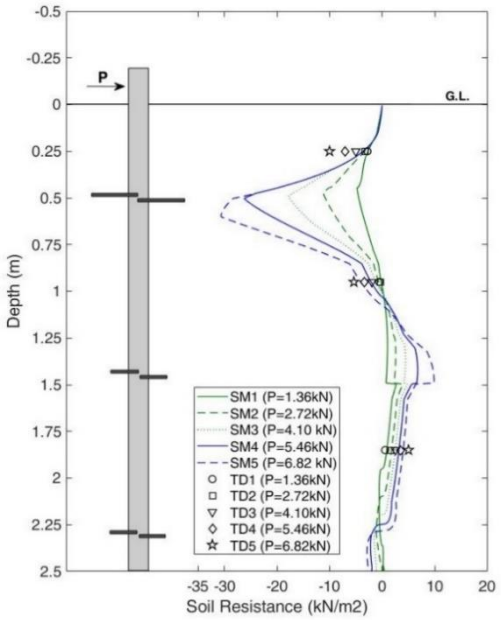

Fig. 11 Simulated vs. measured pile soil resistance

translates until enough shaft soil resistance is mobilized (which is generally further beneath the soil layer, depending on the soil type and its geotechnical properties) to partially restrict the shaft movement, that is why the maximum bending moment of a regular shaft pile is usually around further beneath the soil layer.

The soil resistance in the simulated model has observable spiking values where the helix plate is located. This is only natural and expected due to the added soil resistance provided by the helix plates incorporated to the over-all shaft resistance of the helical pile. The maximum soil resistance is observed to be in the range of 0.5 m ~ 0.6 m below the ground line which is within the region where the helix plate influences. For regular piles, the maximum soil resistance is located in a much lower depth as the pile shaft is still mobilizing adequate soil resistance, while for helical piles, the presence of the helix plates shifts the location of the maximum soil resistance to a closer depth below the ground line (or rather depends on the location of the first helix plate which generally controls the shaft soil resistance of the helical pile). Also observed in the soil resistance distribution for the depths ground line to 0.25 m is that the soil resistance plot for all cases appears to have the same slope until a further increase in depth that the slopes have distinct differences. This can be explained as the maximum soil resistance analytically computed from the soil type and its geotechnical properties in those depths have been reached already. Each discretized spring contains information of p-y curve function for each respective depth, when the maximum soil resistance value is reached, the maximum value is displayed and springs below are being mobilized. It is a rather complex and reiterative process that requires the use of numerical processing. In a general sense, soil resistance increases with depth and the presence of the helix plates further increases the soil resistance the shaft can mobilize in that specific depth.

As shown in Fig. 11, the helical pile has two inflection points (first point is around ~1.1m below the ground line and second point is around ~2.2 m from the ground line) observed which provides an idea of how the soil resistance distribution along the embedded pile length is acting on the helical pile shaft.

Due to the limited field instrumentation, the pile deflection per depth is not shown as it displays unsatisfactory results. This is attributed to the magnified errors from integrating the bending moment curve which requires the solution of integration constants, C_1 and C_2. Due to the flawed curve fitting procedure to approximate the bending moment distribution along the pile, scatter was observed which contributes to data errors. Nip and Ng (2005) suggested that the integration of rotation measurements yields fairly reliable deflection values, their suggestion can be credited to the fact that only one integration constant is needed to satisfy the deflection equation whereas integrating the bending moment measurements would require two integration constants to be solved and contributes to significant errors.

The equations used in this study come from the derived and integrated bending moment measurements recorded during field test. The method suggested by Nip and Ng (2005) could not be used as lack of experiment data could not satisfy the necessary boundary conditions which would lead to the solution of the necessary integration constant to plot the deflection profile of the helical pile.

A numerical simulation was conducted to compare the behavior profile between a helical pile and a regular shaft pile. Both the regular pile and helical pile have an applied load of 5.46 kN and a shaft diameter of 89.1 mm with 3.2 mm wall thickness. The helical pile simulated is fitted with three helices (see Section 3). The soil properties used in this

6. Conclusions

Presented in this research is the characterized lateral behavior of helical piles using modified p-y springs, soil properties from correlated CPT data, and field strain gauge instrumentation. Full scale lateral load tests were conducted with an instrumented helical pile using electrical resistance strain gauges to measure the bending moment of the pile at every load increment. The fourth-order polynomial curve fitting method was used to approximate the developed bending moment along the pile to extract the shear, soil resistance, slope and deflection functions. The measured test results were then compared to the simulated data from a numerical analysis program using the finite difference method and coded in a commercial software, MATLAB. The numerical analysis method was based on the theory of an embedded beam-column element connected to non-linear springs. The springs within the zone of influence are supplemented with p-multipliers to account the presence of helix plates and incorporates its effects to the overall lateral resistance of the shaft.

Established in this study are the following observations and key points in the behavior of a laterally loaded helical pile:

- The geometric configuration of the helical piles mobilize greater lateral resistance compared to regular shaft piles as the latter requires p-multipliers

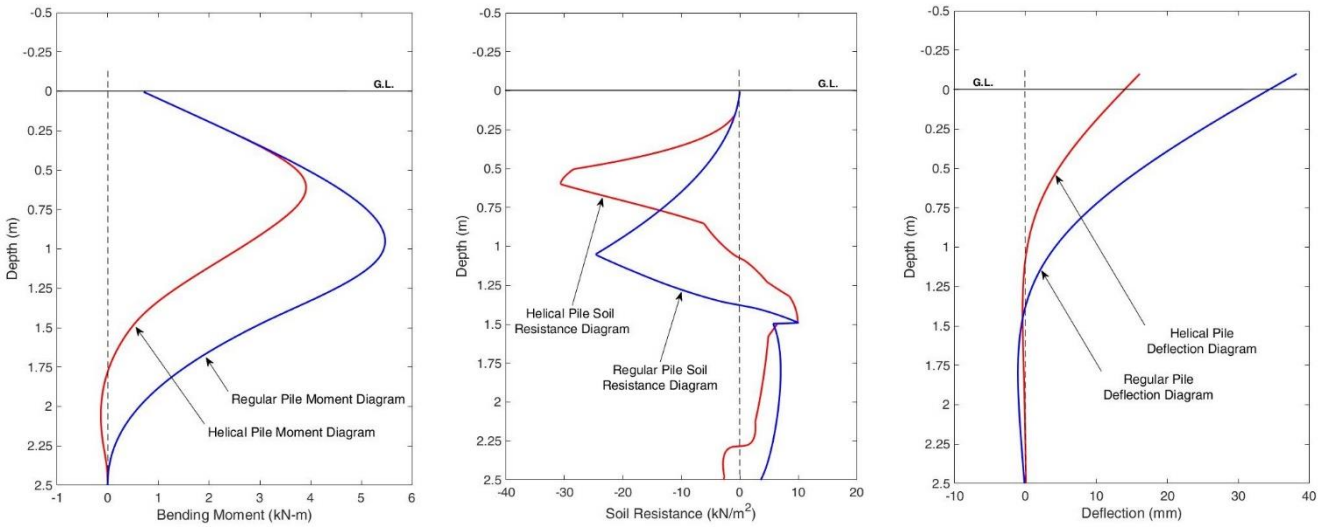

(a) Bending Moment (b) Soil Resistance (c) Deflection

Fig. 12 Comparative behavior profile between a helical pile vs. regular pile

to fit the measured field test results and also from observing the pile head deflection comparison

- There is no general relation for the helix coefficient, it is determined empirically from conducted field experiments and varies from site-to-site depending on the soil type and conditions
- The instrumentation using electrical resistance strain gauges on the test helical piles has captured the embedded lateral behavior and is fairly in agreement with the simulated data
- The predicted lateral displacements generated through the numerical simulation shows fairly in good agreement to the recorded field test results

The results presented in this study should be used with caution and scrutiny when applied for other projects as it depends on the geometrical characteristics of the test pile, site specific and field conditions differ from their respective locations.

Acknowledgments

This research was supported by the Basic Science Research Program through the National Research Foundation of Korea (NRF), funded by the Ministry of Education (NRF2021R1A6A1A1A03045185, Brain Korea 21 FOUR) and by the Human Resources Development of the Korea Institute of Energy Technology Evaluation and Planning (KETEP) grant funded by the Korean government (Ministry of Trade, Industry & Energy) (No.20214000000180)..

References

Abdrabbo, F.M. and El Wakil, A.Z. (2016), "Laterally loaded helical piles in sand", *Alexandria Eng. J.*, **55**(4), 3239-3245. https://doi.org/10.1016/j.aej.2016.08.020.

AC358 (2007), Acceptance criteria for helical foundation systems and devices, ICC-ES (International Code Council–Evaluation Service).

ASTM D3966 (2007), Standard test methods for deep foundations under lateral load. ASTM D3966. West Conshohocken, PA.

Brown, M., Davidson, C., Brennan, A., Knappett, J., Cerfontaine, B. and Sharif, Y. (2019), "Physical modelling of screw piles for offshore wind energy foundations", *Proceedings of the 1st International Symposium on Screw Piles for Energy Applications*. Dundee, United Kingdom, May. https://doi.org/10.20933/382100001123.

Cinicioglu, O. Sancak, E. (2020), "Selection of design friction angle: a strain based empirical method for coarse grained soils", *Geomech. Eng.*, **20**(2), 121-129. https://doi.org/10.12989/gae.2020.20.2.121.

Dave, S. and Soni, M. (2019), "Model tests to determine lateral load capacity of helical piles embedded 384 in sand", *Geotechnics for Transportation Infrastructure*, 529-538. Lecture Notes in Civil 385 Engineering, vol 29. Springer, Singapore. https://doi.org/10.1007/978-981-13-6713-742.

Elkasabgy, M. (2011), "Dynamic and static performance of large-capacity helical piles in cohesive soils", Ph.D. Dissertation, The University of Western Ontario, Canada.

Elkasabgy, M. and El Naggar, M.H. (2019), "Lateral performance and p-y curves for large-capacity helical piles installed in clayey glacial deposit", *J. Geotech. Geoenviron. Eng.*, **145**(10). https://doi.org/10.1061/(ASCE)GT.1943-5606.0002063.

Hetenyi, M. (1946), "Beams on elastic foundation", Scientific Series, vol. XVI. Ann Arbor: The University of Michigan Press, University of Michigan Studies.

Khari, M., Dehghanbandaki, A. and Armaghani, D.J. (2021), "Physical modelling of bending moments in single piles under combined loads in layered soil", *Geomech. Eng.*, **25**(5), 373-381. https://doi.org/10.12989/gae.2021. 25.5.373.

Kim, H.K., Moon, J.S., An, J.W. and Michael, E.S. (2022), "Development of performance evaluation model for road and railway tunnels in use", *Geomech. Eng.*, **29**(3), 369-376. https://doi.org/10.12989/gae.2022.29.3.369.

Kim, H.J., Reyes, J.V., Dinoy, P.R., Park, T.W., Kim, H.S. and Kim, J.Y., (2021), "Modified p-y curves to characterize the lateral behavior of helical piles", *Geomech. Eng.*, **31**(5), 505-518. https://doi.org/10.12989/gae.2022. 31.5.505.

Li, Q. and Yang, Z. (2017), "p-y approach for laterally loaded piles

in frozen silt", *J. Geotech. Geoenviron. Eng.*, **143**(5). https://doi.org/10.1061/(ASCE)GT.1943-5606.0001556.

Lunne, T., Powell, J. and Robertson, P.K. (2002), *Cone penetration testing in geotechnical practice*. CRC Press.

Matlock, H. (1970), "Correlations for design of laterally loaded piles in soft clay", *Proceedings of the 2nd Offshore Technology Conference*, Houston, Texas, 22-24 April 170.

Matlock, H. and Reese, L.C. (1960), "Generalized solutions for laterally loaded piles", *J. Soil Mech. Found. Div. Am. Soc. Civil Engineers*, **86**(5), 63-91.

Matlock, H., Ripperger, E.A. and Fitzgibbon, D.P. (1956), "Static and cyclic lateral-loading of an instrumented pile", Thompson Associates.

Mittal, S., Ganjoo, B. and Shekhar, S. (2010), "Static equilibrium of screw anchor pile under lateral load in sands", *Geotech. Geol. Eng.*, **28**(5), 717-725. https://doi.org/10.1007/s10706-010-9342-4.

Nip, D.C.N. and Ng, C.W.W. (2005), "Back-analysis of laterally loaded bored piles", *Proceedings of the Institution of Civil Engineers-Geotechnical Engineering*, **158**(2), 63-73. https://doi.org/10.1680/geng.2005.158.2.63.

Prasad, Y.V. and Narasimha Rao, S. (1996), "Lateral capacity of helical piles in clays", *J. Geotech. Eng.*, **122**(11), 938-941. https://doi.org/10.1061/(ASCE)0733-9410(19 96)122:11(938).

Puri, V.K., Stephenson, R.W., Dziedzic, E. and Goen, L. (1984), "Helical anchor piles under lateral loading", Laterally loaded deep foundations: Analysis and performance. ASTM International.

Rathod, D., Muthukkumaran, K. and Sitharam, T.G. (2018), "Effect of slope on py curves for laterally loaded piles in soft clay", *Geotech. Geol. Eng.*, **36**(3), 1509-1524. https://doi.org/10.1007/s10706-017-0405-7.

Reese, L.C., Cox, W.R. and Koop, F.D. (1974), "Analysis of Laterally Loaded Piles in Sand", Paper No. OTC 2312, Proceedings of the 7th Offshore Technology Conference, Houston, Texas.

Sakr, M. (2009), "Lateral resistance of helical piles in oil sands", Contemporary Topics in Deep 414 Foundations, 464-471. https://doi.org/10.1061/41021(335)58.

Sakr, M. (2018), "Performance of laterally loaded helical piles in clayey soils established from field experience", *DFI J. Deep Found. Inst.*, **12**(1), 28-41. https://doi.org/10.1080/19375247.2018.1430481.

Seo, M.J., Park, J.B., Lee, D. and Lee, J.S. (2022), "Load-settlement curve combining base and shaft resistance considering curing of cement paste", *Geomech. Eng.*, **29**(4), 407-420. https://doi.org/10.12989/gae.20 22.29.4.407.

Sinha, R., Dave, S.P. and Singh, S.R. (2021), "Lateral performance of helical pile in cohesionless soil", In (Eds., Sitharam, T., Pallepati, R.R. and Kolathayar, S.) Seismic Design and Performance. Lecture Notes in Civil Engineering, **120**. Springer, Singapore. https://doi.org/10.1007/978-981-33-40053 34.

Spagnoli, G. and Tsuha, C. (2020), "A review on the behavior of helical piles as a potential offshore foundation system", *Mar. Georesour. Geotech.*, **38**(9), 1013-1036. https://doi.org/10.1080/1064119X.2020.1729905.

Vignesh, V. and Mayakrishnan, M. (2020), "Design parameters and behavior of helical piles in cohesive soils—A review", *Arabian J. Geosci.*, **13**(22), 1-14. https://doi.org/10.1007/s12517-020-06165-1.